Triad resonance for internal waves in a uniformly stratified fluid: Rogue waves and breathers

H. M. Yin, Q. Pan,[*] and K. W. Chow

Department of Mechanical Engineering, University of Hong Kong, Pokfulam, Hong Kong

Three-wave (triad) resonance in a uniformly stratified fluid is investigated as a case study of energy transfer among oscillatory modes. The existence of a degenerate triad is demonstrated explicitly, where two components have identical group velocity. An illuminating example is a resonance involving waves from modes 1, 3, 5 families, but many other combinations are possible. The physical applications and nonlinear dynamics of rogue waves derived analytically in the literature are examined. Exact solutions with four free parameters (two related to the amplitudes of the background plane waves, two related to the frequencies of slowly varying envelopes) describe motions localized in both space and time. The differences between rogue waves of the degenerate versus the nondegenerate cases are highlighted. The phase and profile of the degenerate case rogue waves are correlated. The volume or energy of the rogue wave (defined as the total extent or energy contents of the fluid set in motion for the duration of the rogue wave) may change drastically, if the wave envelope parameters vary. Pulsating modes (breathers) have been studied previously by layered-fluid and modified Korteweg-de Vries models. Here we extend the consideration to stratified fluids but for the simpler case of nondegenerate triads. Instabilities of fission and fusion of breathers are confirmed computationally with Floquet analysis. This knowledge should prove useful for energy transfer processes in the oceans.

I. INTRODUCTION

Three-wave interactions have been studied intensively in many fields of physical science, e.g. fluids, optics and plasma [1–3]. Significant energy transfers among normal modes under such circumstances have been elucidated theoretically and demonstrated experimentally. Such triadic resonance instability (TRI), also known as three-wave resonance, arises from the strong interactions among three waves. Three-wave resonance occurs when the angular frequency and wave number of one wave component are equal to the sum of angular frequencies and wave numbers of the other two components respectively [4,5]. The governing equations for slowly varying envelopes of three wave trains under resonance condition can be derived by multiple-scale perturbation method. Among the many important applications, we will employ wave propagation in the oceans as an illustrative example.

Internal waves are oscillatory motions propagating within the interior of the oceans. These motions are typically evident along the boundaries of distinct water masses of different densities, or in regions where the density gradients are more abrupt than the surrounding. The energy contained within these waves can cascade from large to small spatial scales, significantly contributing to the mixing and transport processes. These interactions among nonlinear waves have been proposed as one potential mechanism for energy dissipation. Within the context of hydrodynamics, these triadic resonances have also been studied for capillary-gravity water waves [6,7], two-layer systems [8,9], and continuously stratified fluids [10,11]. Long-short resonance constitutes a limiting case of three-wave resonance, where one component is significantly longer than the other two (or alternatively, one wave number is much smaller than the other two). For hydrodynamics, such long wave-short wave interactions have been investigated for a two-layer fluid [12], where two short surface waves are in resonance with a long interfacial wave.

Parametric subharmonic instability (PSI) is a specific case of TRI, where the two secondary waves have lower frequencies than the primary wave. More precisely, small disturbances imposed on the primary wave excite the TRI process, allowing energy to transfer from the primary to the two secondary waves through nonlinearity [3,13]. One case receiving intensive attention occurs when the frequencies of the secondary waves are half of that for the primary wave. PSI mechanisms have been extensively scrutinized in physics, and in particular for internal waves too. As example, the growth rate of PSI for mode-1 waves moving in a uniformly stratified fluid tank has been measured in laboratory experiments and compared with theoretical predictions [14].

Recent investigations have extended considerations to wave beams, examining the influence of carrier wave form on the stability of finite-width wave beams [15,16]. Floquet-type normal mode analysis has been conducted to study the small-scale instability of time-periodic, finite-width internal gravity wave beams in uniformly stratified fluids, both for unbounded domains and channels bounded by rigid walls [17,18]. Experimental evidence demonstrating the impact of TRI on internal wave beams has also been presented [19].

Rogue waves are unexpectedly large displacements from an otherwise tranquil background [20]. For surface gravity waves, there is a sizable literature on theoretical as well as experimental investigations [21,22]. The goal here is to consider if such surprisingly large amplitude motions can occur

---
*Corresponding author: upanqing@connect.hku.hk

in the interior of the oceans too. Laboratory demonstrations of large displacements for stratified fluids will likely be difficult. Field observations and data will probably be even harder to achieve. Nevertheless, preliminary efforts utilizing analytical models of long internal waves have started in the literature [11,23]. Here we study three-wave resonance as a prototype model capturing important aspects of triad dynamics of internal waves of finite wavelengths. For simplicity, we will take a uniformly stratified fluid and make the Boussinesq assumption, i.e., variations in the density of the fluids are ignored except in the buoyancy term of the equations of motion [24].

In addition to rogue waves, breathers (periodic or pulsating modes) in a finite region have also been studied. In particular, breather-like modes can be observed in a layered fluid with a sudden change in bottom topography [25]. Such breathers can also arise in a three-layer fluid model. These pulsating modes can be approximated by the modified Korteweg-de Vries equation, and agree well with direct numerical simulations of the Euler equations [26]. The dynamics of breathers and localized modes can be intriguing, displaying fission and fusion scenarios when the surrounding changes, e.g., varying topography [27,28].

Analytic advances in the studies of rogue waves have proceeded at a tremendous pace in the past decade. Huge varieties of exact solutions have been derived for various classical evolution equations, including the triad resonance case. However, perspectives on the physical applications and nonlinear dynamics of these solutions have not been fully examined, including the present case of the triad resonance system. Our objective is to look into the connection between three-wave resonance in the context of internal waves and the exact solutions from mathematical physics. In particular, we examine a special case of identical group velocity for two of the three modes. The form of the rogue modes will be different from the case with three distinct group velocities.

The structure of the paper can now be explained. We first present the formulation for internal waves in a uniformly stratified fluid. The case of triad resonance with two modes having identical group velocity is explicitly demonstrated (Sec. II). Rogue modes of this degenerate triad resonance (two of the three group velocities being identical) will be tabulated. Their properties, like the displacement, phase and volume, will be delineated (Sec. III). Understanding breathers of the degenerate resonance case may be an elusive goal. Hence we focus on studying breathers for the nondegenerate case first (Sec. IV). Nonlinear dynamics of fission and fusion will be demonstrated. Conclusions will be drawn (Sec. V).

II. FORMULATIONS

A. Existence of degenerate triad for uniform stratification

Consider the wave propagation in an inviscid, incompressible, uniformly stratified fluid with constant buoyancy frequency N_0. The flow is bounded between two rigid walls. Dimensional quantities (those with *) are made dimensionless with reference length scale L, velocity $U_{ref}(=[gL]^{1/2}$, g = gravity) and density ρ_0: $(x, z) = (x^*/L, z^*/L)$, $(u, w) = (u^*/U_{ref}, w^*/U_{ref})$, $t = U_{ref}t^*/L$, $p = p^*/[\rho_0(U_{ref})^2]$, $\rho = \rho^*/\rho_0$. The x^* or z^* axes denote the horizontal or vertical

directions, respectively. We exclude vertical propagation. The nondimensional governing equations [2] are now

$$u_x + w_z = 0, \quad \rho_t + u\rho_x + w\rho_z = 0,$$
$$\rho(u_t + uu_x + wu_z) = -p_x, \quad (1)$$
$$\rho(w_t + uw_x + ww_z) = -p_z - \rho,$$

and the fluid principles are continuity (mass conservation), incompressible flows (material derivative of density being zero), and momentum consideration (pressure gradient being the driving agent for material derivative of momentum). The Boussinesq assumption is made (neglecting the density variations except in the buoyancy term).

Perturbation theory is pursued, by utilizing a small parameter ε being the ratio of the wave amplitude to the channel depth H. The velocity components, density and pressure are expanded in series, with the velocity component u taken as example here:

$$u = \varepsilon \sum_m u_1^{(m)} \exp(i\theta_m) + \varepsilon^2 \sum_m u_2^{(m)} \exp(i\theta_m),$$
$$\theta_m = k_m x - \omega_m t, \quad m = 1, 2, 3, \quad (2)$$

where $m(= 1, 2, 3)$ represents the three components of the triad. We formulate the dynamics as a reduction of the fundamental boundary value problem for internal gravity waves, specifically for high-frequency waves of frequencies far exceeding the local Coriolis parameter [2]. The vertical velocity w and eigenfunction $\Phi(z)$ are then (k_m, ω_m = wave number, angular frequency)

$$(\Phi_m)_{zz} - k_m^2 \Phi_m + \frac{k_m^2}{\omega_m^2} N_0^2 \Phi_m = 0. \quad (3)$$

As the flow is confined between two rigid walls, the boundary conditions will be $\Phi(0) = \Phi(H) = 0$. The corresponding eigenfunction of Eq. (3) is (n = integer, mode number)

$$\Phi_n(z) = \sin(n\pi z/H), \quad (4)$$

with the dispersion relation being

$$\omega_m^2 = \frac{k_m^2 N_0^2}{k_m^2 + \frac{n^2\pi^2}{H^2}}, \quad (5)$$

where $m = 1, 2, 3$, being components of the triad, n = mode number of the internal wave.

The vertical velocity structure is $w_1^{(m)} = E_m(\xi, \tau)\Phi_m(z)$, where $E(\xi, \tau)$ is the slowly varying amplitude. The slow spatial or temporal variables are $\xi = \varepsilon x$, $\tau = \varepsilon t$. The first order $O(\varepsilon)$ terms of the velocity components and density are

$$u_1^{(m)} = \frac{iE_m}{k_m} \frac{d\Phi_m}{dz},$$
$$\rho_1^{(m)} = -\frac{i}{\omega_m} \frac{d\rho(z)}{dz} E_m \Phi_m, \quad (6)$$

where $\rho(z)$ without superscript or subscript stands for the background density. A nonlinear analysis is conducted by substituting the perturbation series [Eq. (2)] into the governing equations [Eq. (1)]. The resonance condition $\boldsymbol{k}_3 = \boldsymbol{k}_1 + \boldsymbol{k}_2$, $\omega_3 = \omega_1 + \omega_2$ is utilized. The inhomogeneous terms for the higher-order perturbations must be orthogonal to the null space of the adjoint operator of Eq. (3), as required by the
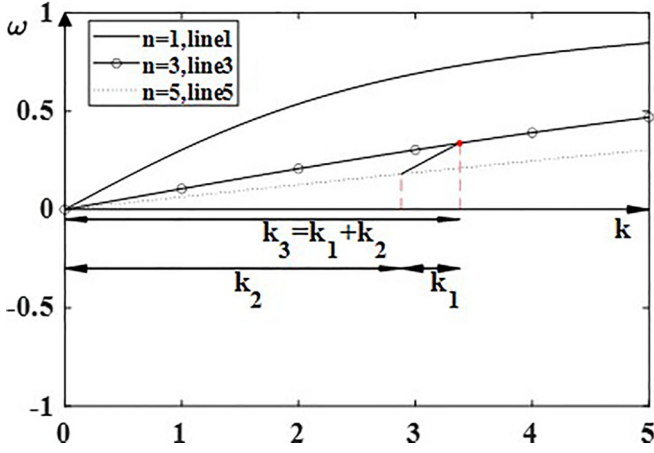
FIG. 1. Graphical construction of a triad.

Fredholm alternative theorem. The evolution equations are then obtained as

$$E_{1\tau} + V_1 E_{1\xi} = r_1 E_3 E_2^*,$$
$$E_{2\tau} + V_2 E_{2\xi} = r_2 E_3 E_1^*,$$
$$E_{3\tau} + V_3 E_{3\xi} = r_3 E_1 E_2, \qquad (7)$$

where V_m $(m = 1, 2, 3)$ are the group velocity of the three members of the triad. The r_m $(m = 1, 2, 3)$ are the corresponding interaction coefficients. Such coefficients can be computed by the standard method of multiple scales [11], but will not be the focus of this work. Instead, we look for special regimes. Equation (7) will be termed a degenerate case when two of the group velocities are identical, i.e., $V_2 = V_3 \neq V_1$. Here we intend to investigate degenerate triads in stratified fluids. As the dispersion relation is given by Eq. (5), one example of triad can be constructed graphically according to the resonance condition in Fig. 1.

As illustrative example, we choose three components coming from the mode number $n = 1, 3, 5$, with modes 1 and 5 being the *daughter wave*, and mode 3 being the *parent wave* ($k_3 = k_1 + k_2$, k_1, k_2 from mode 1 and mode 5, respectively). The terminology of parent and daughter is not uniform in the literature. More precisely,

$$\omega_1^2 = \frac{k_1^2 N_0^2}{k_1^2 + \frac{n_1^2 \pi^2}{H^2}}, \quad \omega_2^2 = \frac{k_2^2 N_0^2}{k_2^2 + \frac{n_2^2 \pi^2}{H^2}}, \quad \omega_3^2 = \frac{k_3^2 N_0^2}{k_3^2 + \frac{n_3^2 \pi^2}{H^2}},$$

$n_1 = 1$, $n_3 = 3$, $n_5 = 5$. Infinitely many sets of triads can be identified among the combinations of the three modes. The
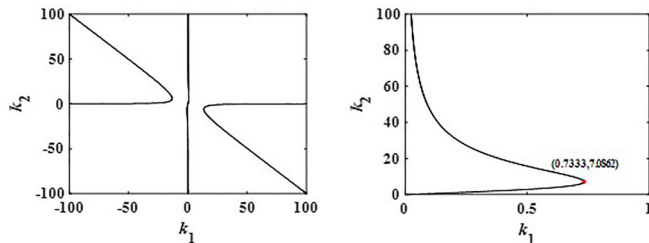

FIG. 2. Existence of triad involving modes 1, 3, and 5 [Eq. (8a)], with $N_0 = 1$, $H = 1$. (Left) Planar plot of allowed values of k_1 and k_2; (Right) Zoom in view for the existence of point of equal group velocity.
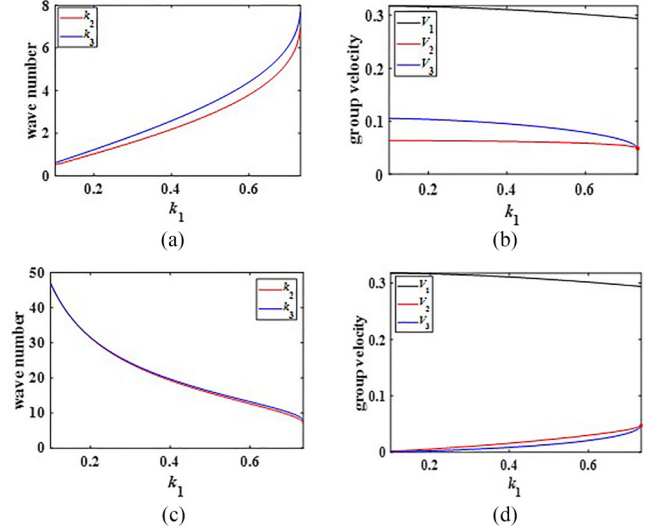

FIG. 3. (a). The variation of the wave number for three components in the first triad set ($k_3 = k_1 + k_2$), with k_1 varying in the interval [0.1, 0.733]; (b). The variation of corresponding group velocity for three components. The parameters chosen are $N_0 = H = 1$; (c), (d) Corresponding properties for the second triad set.

resonance triad can be analytically defined by solving the equation

$$k_1 / \left[k_1^2 + \pi^2 / H^2 \right]^{1/2} + k_2 / \left[k_2^2 + 25\pi^2 / H^2 \right]^{1/2}$$
$$- (k_1 + k_2) / \left[(k_1 + k_2)^2 + 9\pi^2 / H^2 \right]^{1/2} = 0. \quad (8a)$$

For a given water depth H, the solutions for k_1 and k_2 are illustrated (left panel, Fig. 2). For simplicity, the three waves are assumed to propagate in the positive x direction, with k_1, k_2 and k_3 all being positive. For $N_0 = H = 1$, to ensure the existence of a triad, the value of k_1 must be confined within the interval (0, 0.733) (right panel, Fig. 2). For each value of k_1 within this interval, two sets of corresponding values for k_2 and k_3 are permissible. If we vary the water depth H, the trends are qualitatively similar.

To search for the existence of degenerate triads, the variations of wave numbers and the associated group velocities, denoted as $V_m = \frac{\partial \omega_m}{\partial k_m}$ $(m = 1, 2, 3)$ for the three components in these two triad sets are studied (Fig. 3). There is only one degenerate triad for the chosen values of N_0 and H, namely, $k_1 = 0.733$, and $V_2 = V_3 = 0.0481$ [red point in Figs. 3(b) and 3(d)].
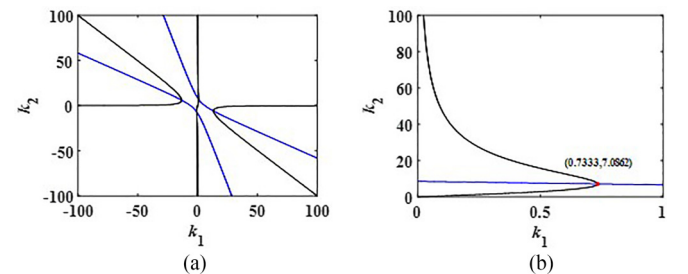

FIG. 4. (a). The full solution graph of k_1 and k_2 to Eq. (8a) (black line) and Eq. (8b) (blue line); (b). The solution graph of positive k_1 and k_2 to Eq. (8a) (black line) and Eq. (8b) (blue line). The parameters chosen are $N_0 = 1$, $H = 1$.

For the existence of a degenerate triad, the group velocities V_2, V_3 must be identical ($\frac{\partial \omega_2}{\partial k_2} = \frac{\partial \omega_3}{\partial k_3}$). From the dispersion relation [Eq. (5)], this condition for the present choice of a resonance among modes 1, 3, 5 is

$$25^4[(k_1 + k_2)^2 + 9\pi^2/H^2]^3 - 9^4[k_2^2 + 25\pi^2/H^2]^3 = 0. \tag{8b}$$

For a given water depth H (=1), the solutions for k_1 and k_2 of Eqs. (8a), (8b) will be illustrated graphically (Fig. 4, black or blue line denoting the solutions to Eqs. (8a) or (8b), respectively). Only four intersection points are observed for $N_0 = H = 1$.

B. Scale transformation

To demonstrate that the degenerate case is theoretically different from the case of distinct group velocities, Eq. (7) can first be reduced to

$$U_{1,T} + V_1^* U_{1,X} = \text{sgn}(s_1) U_3 U_2^*,$$
$$U_{2,T} + V_2^* U_{2,X} = \text{sgn}(s_2) U_3 U_1^*,$$
$$U_{3,T} + V_3^* U_{3,X} = \text{sgn}(s_3) U_1 U_2, \tag{9}$$

where the new system Eq. (9) displays numerically unity interaction coefficients (sgn = sign of the real number). The necessary transformation is

$$T = p_1 \xi + p_2 \tau, \quad X = \xi + p_3 \tau, \tag{10a}$$

$$E_1 = \frac{U_1}{\sqrt{|s_2||s_3|}}, \quad E_2 = \frac{U_2}{\sqrt{|s_1||s_3|}}, \quad E_3 = \frac{U_3}{\sqrt{|s_1||s_2|}}, \tag{10b}$$

$$s_1 = \frac{r_1}{p_2 + V_1 p_1}, \quad s_2 = \frac{r_2}{p_2 + V_2 p_1}, \quad s_3 = \frac{r_3}{p_2 + V_3 p_1}, \tag{10c}$$

$$p_1 = \frac{(V_2 - V_3)V_1^* + (-V_1 + V_3)V_2^* + (V_1 - V_2)V_3^*}{(-V_2 + V_3)V_2^* V_3^* + V_1^*[(-V_1 + V_2)V_2^* + (V_1 - V_3)V_3^*]}, \tag{10d}$$

$$p_2 = \frac{(V_2 - V_3)V_1 V_1^* + (-V_1 + V_3)V_2 V_2^* + (V_1 - V_2)V_3 V_3^*}{(V_2 - V_3)V_2^* V_3^* + V_1^*[(V_1 - V_2)V_2^* + (-V_1 + V_3)V_3^*]}, \tag{10e}$$

$$p_3 = \frac{(-V_2 + V_3)V_1 V_2^* V_3^* + V_1^*[(-V_1 + V_3)V_3 V_2^* + (V_1 - V_3)V_2 V_3^*]}{(V_2 - V_3)V_2^* V_3^* + V_1^*[(V_1 - V_2)V_2^* + (-V_1 + V_3)V_3^*]}, \tag{10f}$$

where V_1^*, V_2^*, V_3^* denote arbitrary constants. This transformation requires that V_1, V_2, V_3 are all different from each other. Hence we can choose arbitrary values of V_1, V_2, V_3 in Eq. (7) as long as they satisfy the relation $V_1 > V_2 > V_3$. For the degenerate case, this inequality cannot hold as $V_2 = V_3 = V$.

III. DYNAMICS OF DEGENERATE TRIADS

A. Contrast between the degenerate and nondegenerate rogue waves

For convenience, we adopt the normalized version of the triad resonance equations [Eq. (7)] by scaling the amplitudes with the interaction coefficients [11]:

$$\phi_{1t} + V_1 \phi_{1x} = \phi_3 \phi_2^*,$$
$$\phi_{2t} + V_2 \phi_{2x} = -\phi_3 \phi_1^*,$$
$$\phi_{3t} + V_3 \phi_{3x} = \phi_1 \phi_2. \tag{11}$$

We focus on rogue events or rogue waves in this paper. Physically, displacements from a tranquil background should be localized in both space and time. Mathematically, analytical solutions for deviations from the background should decay in the far field [20].

The rogue wave solutions for the triad resonance model in the nondegenerate case ($V_1 > V_2 > V_3$) have been given earlier [29–31]. Here, our focus is on triad resonance model in the degenerate case ($V_1 = 0$, $V_2 = V_3 = V$), where two of the three group velocities are identical. The rogue wave mode of Eq. (11) for this degenerate case has been derived in the literature by the Darboux transformation method [32]. We examine the nonlinear dynamics further, and confirm the existence of degenerate resonance in the context of internal waves. More precisely, the rogue waves are given by

$$\phi_1 = i a_1 \exp[i(k_3 - k_2)x - i(\omega_3 - \omega_2)t]\left\{1 - \frac{4i\delta^3 V(Vt - x) + A^2 V^2/a_1^2}{[\delta^2 Vt - (\delta^2 + B)x]^2 + 4\delta^2 a_1^2 x^2 + A^2 V^2/(4a_1^2)}\right\}, \tag{12a}$$

$$\phi_2 = a_2 \exp[i(k_2 x - \omega_2 t)]\left\{1 + \frac{2i\delta V[\delta^2 Vt - (\delta^2 - A)x] - \delta^2 A V^2/a_2^2}{[\delta^2 Vt - (\delta^2 + B)x]^2 + 4\delta^2 a_1^2 x^2 + A^2 V^2/(4a_1^2)}\right\}, \tag{12b}$$

$$\phi_3 = a_3 \exp[i(k_3 x - \omega_3 t)]\left\{1 + \frac{-2i\delta V[\delta^2 Vt - (\delta^2 + A)x] - \delta^2 A V^2/a_3^2}{[\delta^2 Vt - (\delta^2 + B)x]^2 + 4\delta^2 a_1^2 x^2 + A^2 V^2/(4a_1^2)}\right\}, \tag{12c}$$

$$a_1 = \frac{a_3 a_2}{\delta}, \quad k_3 = \frac{\omega_3}{V} + \frac{a_2^2}{\delta V}, \quad k_2 = \frac{\omega_2}{V} + \frac{a_3^2}{\delta V}, \tag{12d}$$

$$A = a_3^2 + a_2^2, \quad B = a_3^2 - a_2^2, \quad \kappa = \omega_3 + \omega_2, \quad \delta = \omega_3 - \omega_2. \tag{12e}$$
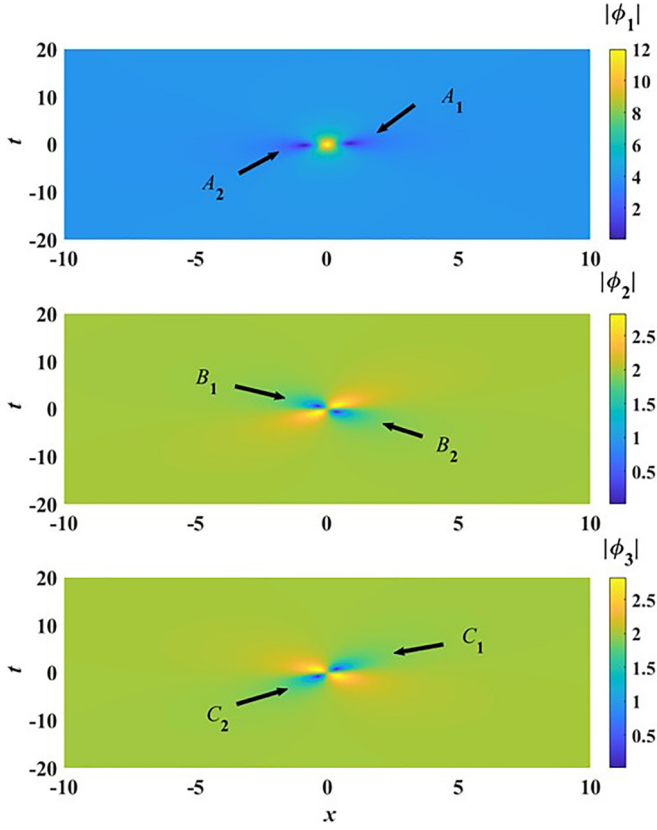
FIG. 5. Rogue waves with parameters $a_2 = 2$, $a_3 = 2$, $\omega_2 = 1$, $\omega_3 = 2$, $V = 4$.

Here the amplitudes of the plane waves for the three components, namely a_1, a_2, a_3, serve as benchmarks where maximum displacements of the rogue waves can be compared. Given a group velocity V, Eq. (12) represents a family of solutions with four free parameters (a_2, a_3, ω_2, ω_3). Before proceeding further, we must emphasize on the difference between the rogue waves of the degenerate and the nondegenerate triad resonance. Rather than going through lengthy comparisons and manipulations of mathematical ex-

pressions, we will just illustrate the contrast graphically. Basically, the rogue wave profiles differ drastically with fixed amplitudes of plane wave background (parameters a_2, a_3) and angular frequencies of the carrier wave envelopes (parameters ω_2, ω_3). Details are described in the Appendix A.

B. Displacement and phase of the rogue waves

It is instructive to inspect the location and magnitude of the largest displacements of the rogue waves for the degenerate case. The ϕ_1 component displays an eye-shaped pattern (a peak accompanied by two valleys on the two opposite sides), while the components ϕ_2, ϕ_3 exhibit a four-petal profile (two peaks and two valleys with a saddle point in the center) [33]. In terms of naming, we term the depth of the valley as the minimum displacement (smallest distance to the plane defined by vertical coordinate being zero). The minimum displacements for the three components are located at points A_1, A_2, B_1, B_2, C_1, C_2 as labeled in Fig. 5. The precise spatial and temporal coordinates are tabulated (Table I).

We now turn our attention to the phase of the rogue waves. For convenience, the exponential factor with modulus unity is removed to highlight the nonlinear dynamics [Eq. (12)]. The rational portions of the rogue wave solutions are

$$\hat{\phi}_1 = 1 - \frac{4i\delta^3 V(Vt - x) + A^2 V^2/a_1^2}{[\delta^2 Vt - (\delta^2 + B)x]^2 + 4\delta^2 a_1^2 x^2 + A^2 V^2/(4a_1^2)}, \tag{13a}$$

$$\hat{\phi}_2 = 1 + \frac{2i\delta V[\delta^2 Vt - (\delta^2 - A)x] - \delta^2 A V^2/a_2^2}{[\delta^2 Vt - (\delta^2 + B)x]^2 + 4\delta^2 a_1^2 x^2 + A^2 V^2/(4a_1^2)}, \tag{13b}$$

$$\hat{\phi}_3 = 1 + \frac{-2i\delta V[\delta^2 Vt - (\delta^2 + A)x] - \delta^2 A V^2/a_3^2}{[\delta^2 Vt - (\delta^2 + B)x]^2 + 4\delta^2 a_1^2 x^2 + A^2 V^2/(4a_1^2)}. \tag{13c}$$

The phase factors of the three complex valued components are

$$\psi_1 = \arctan\left\{\frac{-4\delta^3 V(Vt - x)}{[\delta^2 Vt - (\delta^2 + B)x]^2 + 4\delta^2 a_1^2 x^2 + A^2 V^2/(4a_1^2) - A^2 V^2/a_1^2}\right\}, \tag{14a}$$

$$\psi_2 = \arctan\left\{\frac{2\delta V[\delta^2 Vt - (\delta^2 - A)x]}{[\delta^2 Vt - (\delta^2 + B)x]^2 + 4\delta^2 a_1^2 x^2 + A^2 V^2/(4a_1^2) - \delta^2 A V^2/a_2^2}\right\}, \tag{14b}$$

$$\psi_3 = \arctan\left\{\frac{-2\delta V[\delta^2 Vt - (\delta^2 + A)x]}{[\delta^2 Vt - (\delta^2 + B)x]^2 + 4\delta^2 a_1^2 x^2 + A^2 V^2/(4a_1^2) - \delta^2 A V^2/a_3^2}\right\}. \tag{14c}$$

The phase of the rogue wave is shown to correlate strongly with the nonlinear dynamics (Fig. 6). We can identify the minimum displacements of the rogue wave profiles, along the directions of the white dotted lines passing through points A_1, A_2, B_1, B_2, C_1, C_2 as indicated in Table I. The peak of the component ϕ_1 is attained at the point $x = t = 0$. Those

white lines indeed pass through this peak. The expressions of the white dotted lines can be determined by the relations between x and t (black texts in Fig. 6), where the slopes are derived from the spatial and temporal coordinates in Table I. The precise relations will change numerically with different input parameters such as a_2, a_3, ω_2, ω_3, and V. For the widely

TABLE I. Spatial and temporal locations of minimum displacements of the three components.

Components	Points of minimum displacements in Fig. 5	Spatial and temporal locations in Fig. 5	Expressions of white dotted lines (Fig. 6)
ϕ_1	A_1	$x = 0.87,\ t = 0.22$	$t = 0.253\,x$
	A_2	$x = -0.87,\ t = -0.22$	
ϕ_2	B_1	$x = -0.35,\ t = 0.62$	$t = -1.771\,x$
	B_2	$x = 0.35,\ t = -0.62$	
ϕ_3	C_1	$x = 0.35,\ t = 0.79$	$t = 2.257x$
	C_2	$x = -0.35,\ t = -0.79$	

studied nonlinear Schrödinger equation case, the rogue wave profile is obtained by setting the propagation variable to be zero [20,32]. The rogue wave profiles along the white dotted lines are illustrated in the top panel of Fig. 7. Both the amplitude and width of the rogue mode for the component ϕ_1 are larger than those for the ϕ_2 and ϕ_3 components. The maximum amplitude of the ϕ_1 component [Eq. (12)] occurs at $x = 0$, $t = 0$ (Fig. 5), and is three times its mean state or tranquil background (a_1). The corresponding magnification ratios for the ϕ_2 and ϕ_3 components are smaller. There is a phase shift of π ($\Delta\psi_j,\ j = 1,\ 3$) between the continuous wave background and the central part of the components for ϕ_1 and ϕ_3 (the middle panel of Fig. 7). For the component ϕ_2, there is a $-\pi$ phase shift ($\Delta\psi_2$) along the direction of the white dotted line. The maximum phase shift is 2π (Fig. 6). To find out the direction of the maximum phase shift, we define

the temporal evolution of phase shift $\Delta\psi_j(j = 1,\ 2,\ 3)$ as

$$\Delta\psi_j(t) = \psi_j(t, x = 0) - \psi_j(t, x \to \infty), \quad j = 1,\ 2,\ 3. \tag{15}$$

The temporal evolution of $\Delta\psi_j$ can be obtained analytically by

$$\tan(\Delta\psi_1) = -\frac{4\delta^3 V^2 t}{\delta^4 V^2 t^2 + A^2 V^2/(4a_1^2) - A^2 V^2/a_1^2},$$

$$\tan(\Delta\psi_2) = \frac{2\delta^3 V^2 t}{\delta^4 V^2 t^2 + A^2 V^2/(4a_1^2) - \delta^2 A V^2/a_2^2},$$

$$\tan(\Delta\psi_3) = -\frac{2\delta^3 V^2 t}{\delta^4 V^2 t^2 + A^2 V^2/(4a_1^2) - \delta^2 A V^2/a_3^2}, \tag{16}$$
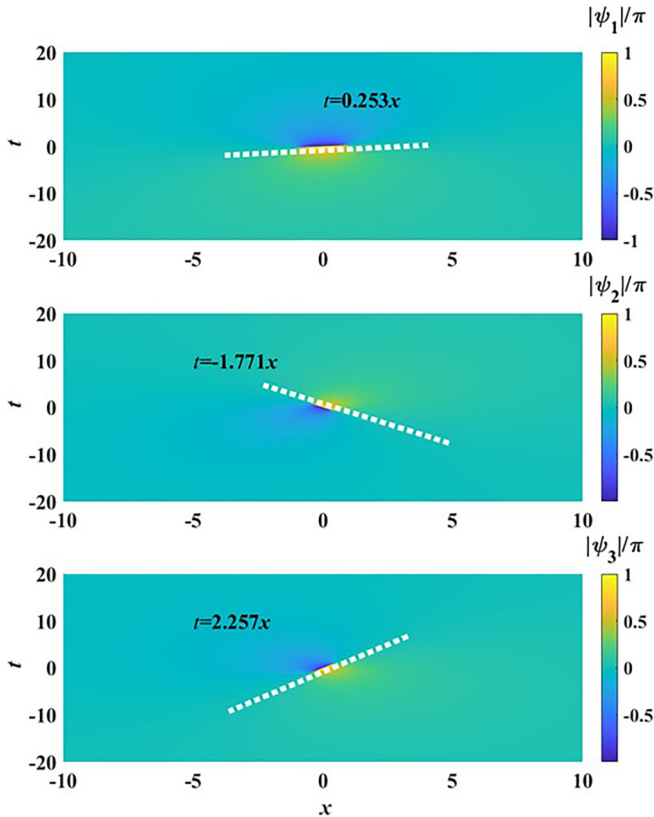

FIG. 6. Phase of the rogue waves versus x and t: White dotted lines denoting the minimum amplitude of the rogue wave. Parameters chosen are $a_2 = 2$, $a_3 = 2$, $\omega_2 = 1$, $\omega_3 = 2$, $V = 4$.
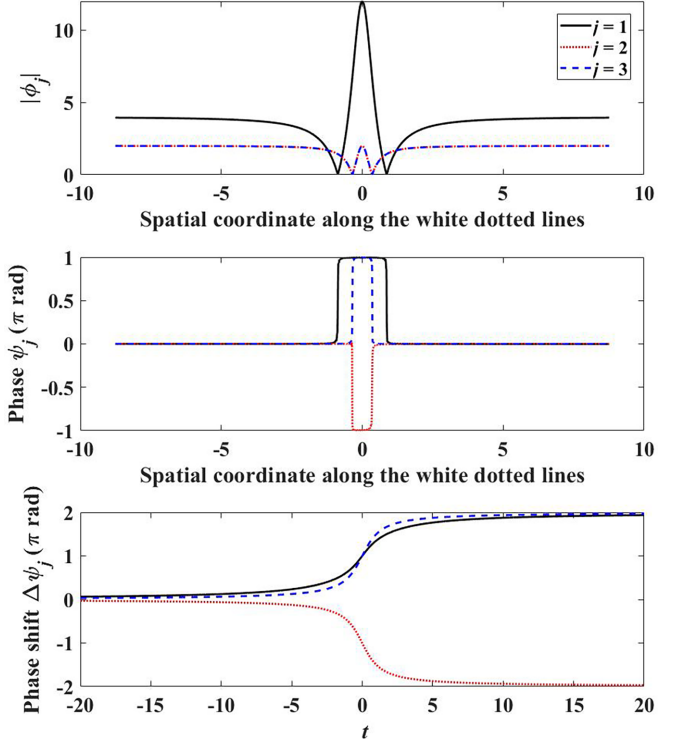

FIG. 7. Top panel: Rogue wave profile in the direction denoted by the white dotted lines; Middle panel: Phase profile along the white dotted lines of Fig. 6; Bottom panel: Evolution of the phase shift between the central part and the continuous background (the phase has been unwrapped). Parameters chosen are $a_2 = 2$, $a_3 = 2$, $\omega_2 = 1$, $\omega_3 = 2$, $V = 4$.
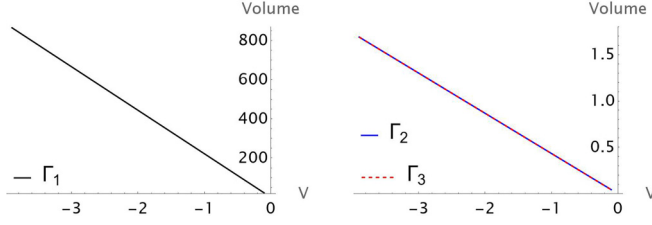
FIG. 8. Volumes of the three components versus the group velocity V with parameters $a_2 = \sqrt{3}$, $a_3 = 1$, $\omega_2 = 1$, $\omega_3 = 0.5$.

which is illustrated in the bottom panel of Fig. 7. For the three components of the rogue waves in triad resonance, there is a phase excursion of 2π. This feature is also observed for the Peregrine breather and the Fermi-Pasti-Ulam-Tsingou recurrence in the widely studied nonlinear Schrödinger equation [34,35].

C. Volume or energy of the rogue wave

For rogue waves of triads, it is instructive to examine the extent of fluid displaced for the whole spatial domain over the duration of occurrence. For such calculations, we draw an analogy with the rogue modes of the surface wave counterparts, where slowly varying packets are governed by the nonlinear Schrödinger equation. Along this line of reasoning, we define the volume of each component as [36]

$$\Gamma_1 = \frac{1}{8\pi} \int_{-\infty}^{\infty} \int_{-\infty}^{\infty} \left(|\phi_1|^2 - a_1^2 \right)^2 dx dt,$$

$$\Gamma_2 = \frac{1}{8\pi} \int_{-\infty}^{\infty} \int_{-\infty}^{\infty} \left(|\phi_2|^2 - a_2^2 \right)^2 dx dt,$$

$$\Gamma_3 = \frac{1}{8\pi} \int_{-\infty}^{\infty} \int_{-\infty}^{\infty} \left(|\phi_3|^2 - a_3^2 \right)^2 dx dt, \tag{17}$$

where the integrals are evaluated with ϕ_n, $n = 1, 2, 3$ given by the exact solutions [Eq. (12)]. Depending on the basic physical principles under study, Eq. (17) may be mapped to the energy of the system. Such definitions can in principle be correlated with the potential damage the rogue wave can inflict on a ship, offshore or submerged structure.

The volumes of the rogue waves are now scrutinized as the input parameters vary. These volumes of the three components are inversely proportional to the group velocity V. The rate of decrease in the volume of the component ϕ_1 as the daughter wave is larger than those of the components ϕ_2 and ϕ_3 (Fig. 8). The difference between the frequencies of the carrier envelope of components ϕ_2 and ϕ_3 can significantly affect the volumes of the three components (Fig. 9). As the frequencies of ϕ_2
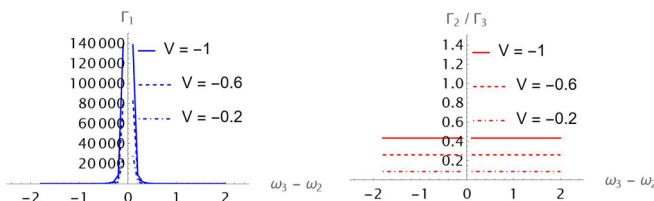

FIG. 9. Volumes of the three components versus the difference in angular frequencies of the carrier envelopes $\omega_3 - \omega_2$.
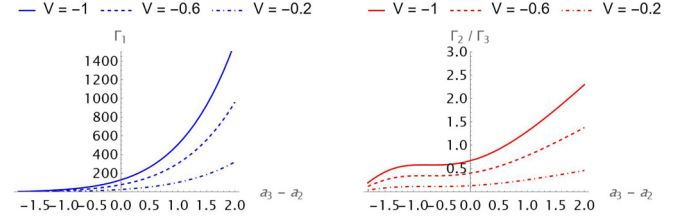

FIG. 10. Volumes of the three components versus the difference in amplitudes of the carrier envelopes $a_3 - a_2$.

and ϕ_3 approach each other, the volume of ϕ_1 can increase dramatically. The volumes of ϕ_2 and ϕ_3 remain unchanged as the difference between their frequencies varies. Figure 9 displays a divergent behavior at the point of $\omega_3 - \omega_2 = 0$ (or $\omega_3 = \omega_2$), as degenerate triad resonance cannot exist in that case [$\delta \to 0$ will imply k_2, $k_3 \to \infty$, Eqs. (12d) and (12e)]. The difference in amplitudes between ϕ_2 and ϕ_3 also has a significant effect on the volumes of the three components (Fig. 10). The volumes of all three components increase with a larger difference in amplitudes.

IV. DYNAMICS OF NONDEGENERATE TRIADS

For the widely studied nonlinear Schrödinger equation, rogue waves can only occur in the focusing regime, where there is long wavelength modulation instability. Similar insight on instabilities and rogue waves or breathers also holds for coupled Schrödinger type waveguides [33]. Remarkably, these connections between instability and the occurrence of extreme events also remain valid for the triad resonance case. Linear instabilities of the baseband (long wavelength) type still serve as a critical condition for the emergence of rogue waves [37].

Theoretically rogue waves are studied with decaying boundary conditions in an unbounded field. For a finite domain with periodic boundary conditions, the analog is then a breather. While breathers for surface waves have been investigated, the corresponding properties for internal waves and triad resonance are only beginning to be realized. For this purpose, pulsating modes for the nondegenerate case are studied here first. Fission and fusion phenomena are demonstrated. More detailed description of dynamics and properties of breathers for the degenerate case will be deferred to a future work.

The analytical techniques involved are the Darboux transformation and the Lax pair. The Darboux transformation defines a recursive process where more complicated solutions can be generated from simpler ones (seed solutions). The Lax pair introduces the time and space dependence of auxiliary functions and eigenvalues. This mechanism started in the 1960s in the search of analytic advances of the Korteweg–de Vries and Schrödinger equations.

In a previous work, we have initiated investigations on the Fermi-Pasta-Ulam-Tsingou recurrence phenomena of breathers of the triad systems [38]. Basically, small disturbances on a plane wave background are amplified due to modulation instability. Higher harmonics exponentially small initially will grow at a higher rate. Eventually all modes attain roughly the same magnitude and a breather is formed at that

instant. Here we demonstrate further intriguing properties of breathers by showing the scenarios of fusion and fission.

A. Breather fission or fusion

The normalized resonant triad system [Eq. (11)] with $V_1 > V_2 > 0$, $V_3 = 0$ (without loss of generality), admits the plane wave system as background

$$\phi_1^{[0]} = \delta_1 \exp[i(k_1 x + q_1 t)],$$

$$\phi_2^{[0]} = \delta_2 \exp[i(k_2 x + q_2 t)],$$

$$\phi_3^{[0]} = -i\delta_3 \exp[i(k_1 + k_2)x + i(q_1 + q_2)t], \quad (18)$$

where the parameters are given by

$$q_1 = -\frac{k_1 V_1 \delta_1 + \delta_2 \delta_3}{\delta_1},$$

$$q_2 = \frac{-V_3 \delta_1^2 \delta_3^2 + V_2 \delta_2 \left[\delta_1^2 \delta_2 + k_1 (V_1 - V_3) \delta_1 \delta_3 + \delta_2 \delta_3^2 \right]}{(V_2 - V_3) \delta_1 \delta_2 \delta_3},$$

$$k_2 = \frac{-\delta_1^2 \delta_2^2 + k_1(-V_1 + V_3)\delta_1 \delta_2 \delta_3 + (\delta_1 - \delta_2)(\delta_1 + \delta_2)\delta_3^2}{(V_2 - V_3)\delta_1 \delta_2 \delta_3}. \quad (19)$$

The triad system Eq. (11) is integrable. It allows a Lax pair formulation [1,38,39] given as follows:

$$\Psi_x = \mathbf{U}\Psi, \quad \Psi_t = \mathbf{V}\Psi, \quad (20)$$

where $\Psi(x, t) = (\psi_1, \psi_2, \psi_3)^T$ is a 3×1 column vector (superscript T = transpose). The matrices $\mathbf{U}(x, t)$ and $\mathbf{V}(x, t)$ are given by [38]

$$\mathbf{U} = \begin{pmatrix} -\frac{i}{3}(-2V_1 + V_2 + V_3)\lambda & \frac{\phi_3^*(x,t)}{\sqrt{(V_1-V_3)(V_2-V_3)}} & -\frac{\phi_2^*(x,t)}{\sqrt{(V_1-V_2)(V_2-V_3)}} \\ -\frac{\phi_3(x,t)}{\sqrt{(V_1-V_3)(V_2-V_3)}} & -\frac{i}{3}(V_1 - 2V_2 + V_3)\lambda & \frac{\phi_1(x,t)}{\sqrt{(V_1-V_2)(V_1-V_3)}} \\ \frac{\phi_2(x,t)}{\sqrt{(V_1-V_2)(V_2-V_3)}} & -\frac{\phi_1^*(x,t)}{\sqrt{(V_1-V_2)(V_1-V_3)}} & -\frac{i}{3}(V_1 + V_2 - 2V_3)\lambda \end{pmatrix}, \quad (21a)$$

$$\mathbf{V} = \begin{pmatrix} \frac{i}{3}(-V_1 V_2 - V_1 V_3 + 2V_2 V_3)\lambda & -\frac{V_3 \phi_3^*(x,t)}{\sqrt{(V_1-V_3)(V_2-V_3)}} & \frac{V_2 \phi_2^*(x,t)}{\sqrt{(V_1-V_2)(V_2-V_3)}} \\ \frac{V_3 \phi_3(x,t)}{\sqrt{(V_1-V_3)(V_2-V_3)}} & \frac{i}{3}(-V_1 V_2 + 2V_1 V_3 - V_2 V_3)\lambda & -\frac{V_1 \phi_1(x,t)}{\sqrt{(V_1-V_2)(V_1-V_3)}} \\ -\frac{V_2 \phi_2(x,t)}{\sqrt{(V_1-V_2)(V_2-V_3)}} & \frac{V_1 \phi_1^*(x,t)}{\sqrt{(V_1-V_2)(V_1-V_3)}} & \frac{i}{3}(2V_1 V_2 - V_1 V_3 - V_2 V_3)\lambda \end{pmatrix}, \quad (21b)$$

and λ is a complex valued spectral variable. A constraint on the group velocities, i.e., $V_1 > V_2 > V_3$, should hold. The Darboux transformation [38,39] for Eq. (11) can be written as

$$\phi_1^{[1]} = \phi_1^{[0]} - \frac{i(\lambda^* - \lambda)\sqrt{(V_1 - V_2)(V_1 - V_3)}(V_2 - V_3)\psi_2 \psi_3^*}{\psi_1 \psi_1^* + \psi_2 \psi_2^* + \psi_3 \psi_3^*}, \quad (22a)$$

$$\phi_2^{[1]} = \phi_2^{[0]} - \frac{i(\lambda^* - \lambda)\sqrt{(V_1 - V_2)(V_2 - V_3)}(V_3 - V_1)\psi_1^* \psi_3}{\psi_1 \psi_1^* + \psi_2 \psi_2^* + \psi_3 \psi_3^*}, \quad (22b)$$

$$\phi_3^{[1]} = \phi_3^{[0]} + \frac{i(\lambda - \lambda^*)\sqrt{(V_1 - V_3)(V_2 - V_3)}(V_1 - V_2)\psi_1^* \psi_2}{\psi_1 \psi_1^* + \psi_2 \psi_2^* + \psi_3 \psi_3^*}. \quad (22c)$$

To obtain the breather modes, we set the transformation

$$\Psi = G \,\Xi, \quad (23)$$

with the 3×3 nonsingular matrix

$$G = \begin{pmatrix} \exp\left[i(k_1 x + q_1 t)\right] & 0 & 0 \\ 0 & \exp\left[i(k_2 x + q_2 t)\right] & 0 \\ 0 & 0 & \exp\left[i(k_1 x + q_1 t) + i(k_2 x + q_2 t)\right] \end{pmatrix}. \tag{24}$$

Utilizing Eqs. (20) and (23), we derive

$$\begin{aligned} \Xi_x &= \left(G^{-1}\mathbf{U}G + G_x^{-1}G\right)\Xi = \mathbf{U}_0\Xi, \\ \Xi_t &= \left(G^{-1}\mathbf{V}G + G_t^{-1}G\right)\Xi = \mathbf{V}_0\Xi, \end{aligned} \tag{25}$$

where

$$\mathbf{U}_0 = \begin{pmatrix} -\frac{i}{3}(-2V_1 + V_2)\lambda & \frac{i}{\sqrt{V_1 V_2}} & -\frac{1}{\sqrt{(V_1 - V_2)V_2}} \\ \frac{i}{\sqrt{V_1 V_2}} & \frac{i}{V_2} - \frac{i}{3}(V_1 - 2V_2)\lambda & \frac{1}{\sqrt{V_1(V_1 - V_2)}} \\ \frac{1}{\sqrt{(V_1 - V_2)V_2}} & -\frac{1}{\sqrt{V_1(V_1 - V_2)}} & \frac{i}{V_2} - \frac{i}{3}(V_1 + V_2)\lambda \end{pmatrix}, \tag{26a}$$

$$\mathbf{V}_0 = \begin{pmatrix} -\frac{i}{3}(3 + V_1 V_2\lambda) & 0 & \frac{V_2}{\sqrt{(V_1 - V_2)V_2}} \\ 0 & -\frac{i}{3}(6 + V_1 V_2\lambda) & -\frac{V_1}{\sqrt{V_1(V_1 - V_2)}} \\ -\frac{V_2}{\sqrt{(V_1 - V_2)V_2}} & \frac{V_1}{\sqrt{V_1(V_1 - V_2)}} & \frac{i}{3}(-9 + 2V_1 V_2\lambda) \end{pmatrix}. \tag{26b}$$

Combining Eqs. (23) and (25), the solution for the Lax pair (20) can be obtained as

$$\Psi = Q_1 + Q_2 + Q_3, \tag{27}$$

where Q_1, Q_2, Q_3 are expressed in terms of the eigenvalues and eigenvectors of $\mathbf{U}_0$. Details on the calculations of Q_1, Q_2, Q_3 are given in Appendix B.

The fission and fusion processes can now be illustrated using typical input parameters. The left column of Fig. 11 displays the breather fission phenomenon, where a breather splits into two breathers, with the typical parameters $\delta_1 = 1$, $\delta_2 = 1$, $\delta_3 = 1$, $k_1 = 0$, $\lambda = -1 + i$, $V_3 = 0$, $V_2 = 1$, $V_1 = 2$. The period of first breather along t axis is 4. Breather fusion can be obtained by the same parameters as above except for the opposite imaginary part of the eigenvalue, λ.

B. Floquet analysis

We examine the stabilities of breather fission and fusion by the Floquet analysis [40]. Small perturbations ξ_j, $j = 1, 2, 3$, are imposed on the breather solutions

$$\phi_1(x, t) = \phi_{1,\text{bre}}(x, t) + \varepsilon\xi_1(x, t), \quad \phi_2(x, t) = \phi_{2,\text{bre}}(x, t) + \varepsilon\xi_2(x, t), \quad \phi_3(x, t) = \phi_{3,\text{bre}}(x, t) + \varepsilon\xi_3(x, t), \tag{28}$$

where ε is a small parameter. Substituting Eq. (28) into Eq. (11), we obtain the linear equation of $\xi_j(x, t)$ (for $\varepsilon \ll 1$)

$$\begin{aligned} \xi_{1,t}(x, t) + V_1\xi_{1,x}(x, t) - \phi_{3,\text{bre}}(x, t)\xi_2^*(x, t) - \phi_{2,\text{bre}}^*(x, t)\xi_3(x, t) &= 0, \\ \xi_{2,t}(x, t) + V_2\xi_{2,x}(x, t) + \phi_{3,\text{bre}}(x, t)\xi_1^*(x, t) + \phi_{1,\text{bre}}^*(x, t)\xi_3(x, t) &= 0, \\ \xi_{3,t}(x, t) + V_3\xi_{3,x}(x, t) - \phi_{1,\text{bre}}(x, t)\xi_2(x, t) - \phi_{2,\text{bre}}(x, t)\xi_1(x, t) &= 0. \end{aligned} \tag{29}$$

With this transformation

$$\xi_1 = \xi_{1R} + i\xi_{1I}, \quad \xi_2 = \xi_{2R} + i\xi_{2I}, \quad \xi_3 = \xi_{3R} + i\xi_{3I}, \tag{30}$$

Eq. (29) can be separated into the real and imaginary parts

$$\begin{aligned} \xi_{1R,t} + V_1\xi_{1R,x} - \phi_{3,\text{bre}}\xi_{2R} - \phi_{2,\text{bre}}^*\xi_{3R} &= 0, & \xi_{1I,t} + V_1\xi_{1I,x} + \phi_{3,\text{bre}}\xi_{2I} - \phi_{2,\text{bre}}^*\xi_{3I} &= 0, \\ \xi_{2R,t} + V_2\xi_{2R,x} + \phi_{3,\text{bre}}\xi_{1R} + \phi_{1,\text{bre}}^*\xi_{3R} &= 0, & \xi_{2I,t} + V_2\xi_{2I,x} - \phi_{3,\text{bre}}\xi_{1I} + \phi_{1,\text{bre}}^*\xi_{3I} &= 0, \\ \xi_{3R,t} + V_3\xi_{3R,x} - \phi_{2,\text{bre}}\xi_{1R} - \phi_{1,\text{bre}}\xi_{2R} &= 0, & \xi_{3I,t} + V_3\xi_{3I,x} - \phi_{2,\text{bre}}\xi_{1I} - \phi_{1,\text{bre}}\xi_{2I} &= 0, \end{aligned} \tag{31}$$

which can be rewritten as

$$
Z_t = \begin{pmatrix}
-V_1\partial_x & 0 & \phi_{3,\text{bre}} & 0 & \phi_{2,\text{bre}}^* & 0 \\
0 & -V_1\partial_x & 0 & -\phi_{3,\text{bre}} & 0 & \phi_{2,\text{bre}}^* \\
-\phi_{3,\text{bre}} & 0 & -V_2\partial_x & 0 & -\phi_{1,\text{bre}}^* & 0 \\
0 & \phi_{3,\text{bre}} & 0 & -V_2\partial_x & 0 & -\phi_{1,\text{bre}}^* \\
\phi_{2,\text{bre}} & 0 & \phi_{1,\text{bre}} & 0 & -V_3\partial_x & 0 \\
0 & \phi_{2,\text{bre}} & 0 & \phi_{1,\text{bre}} & 0 & -V_3\partial_x
\end{pmatrix} Z = H(x)Z,
\tag{32}
$$

with the entries defined by

$$
Z = (\xi_{1R}, \quad \xi_{1I}, \quad \xi_{2R}, \quad \xi_{2I}, \quad \xi_{3R}, \quad \xi_{3I})^T.
\tag{33}
$$

The monodromy matrix $H(x)$ is periodic in the t direction. The classical Floquet theory for differential equations with periodic coefficients confirms that Eq. (32) can be solved by

$$
Z(t + T) = Z(t)Z^{-1}(0)Z(T).
\tag{34}
$$

The monodromy matrix is then given by $H = Z^{-1}(0)Z(T)$. We can also derive the solution of Eq. (32) as

$Z(t) = \Lambda(t)\exp(Rt)$ by the Floquet theorem, where R is a constant matrix and $\Lambda(t)$ is periodic. Because of the periodicity of $\Lambda(t)$, we have

$$
\begin{aligned}
Z(t + T) &= \Lambda(t + T)\exp[R(t + T)] \\
&= \Lambda(t)\exp[R(t + T)] = Z(t)\exp(RT).
\end{aligned}
\tag{35}
$$

From Eqs. (34) and (35), the following formula:
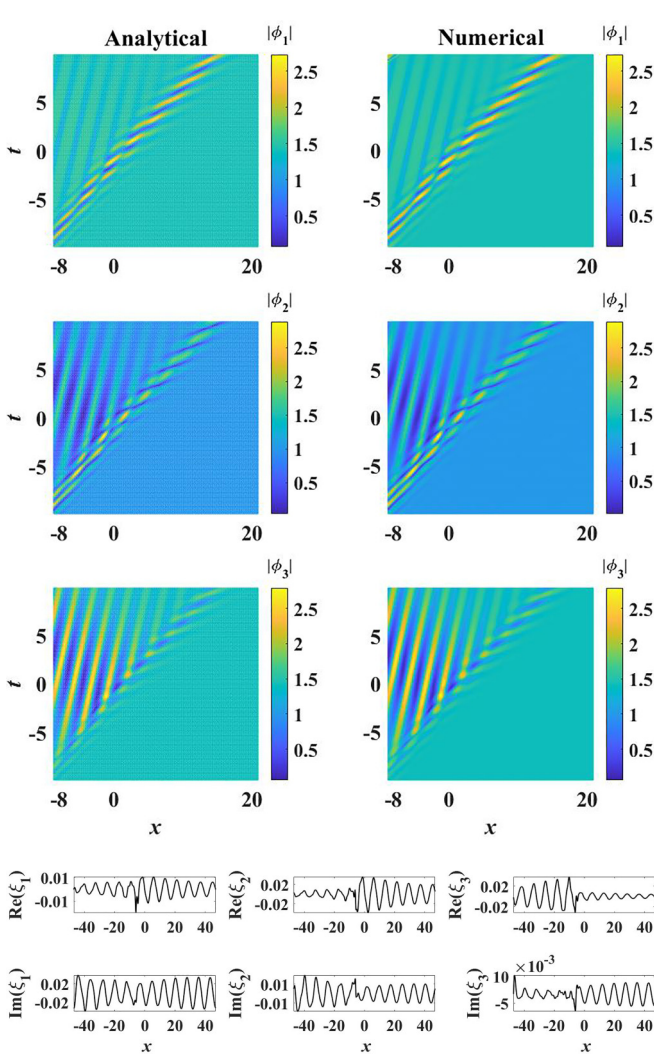
$$
H = Z^{-1}(0)Z(T) = \exp(RT),
\tag{36}
$$

FIG. 11. (Top) Fission of breather; (Bottom) Eigenvectors by Floquet analysis. Parameters values: $\delta_1 = \delta_2 = \delta_3 = 1$, $k_1 = 0$, $\lambda = -1 + i$, $V_3 = 0$, $V_2 = 1$, $V_1 = 2$, $\mu = 0.01$.
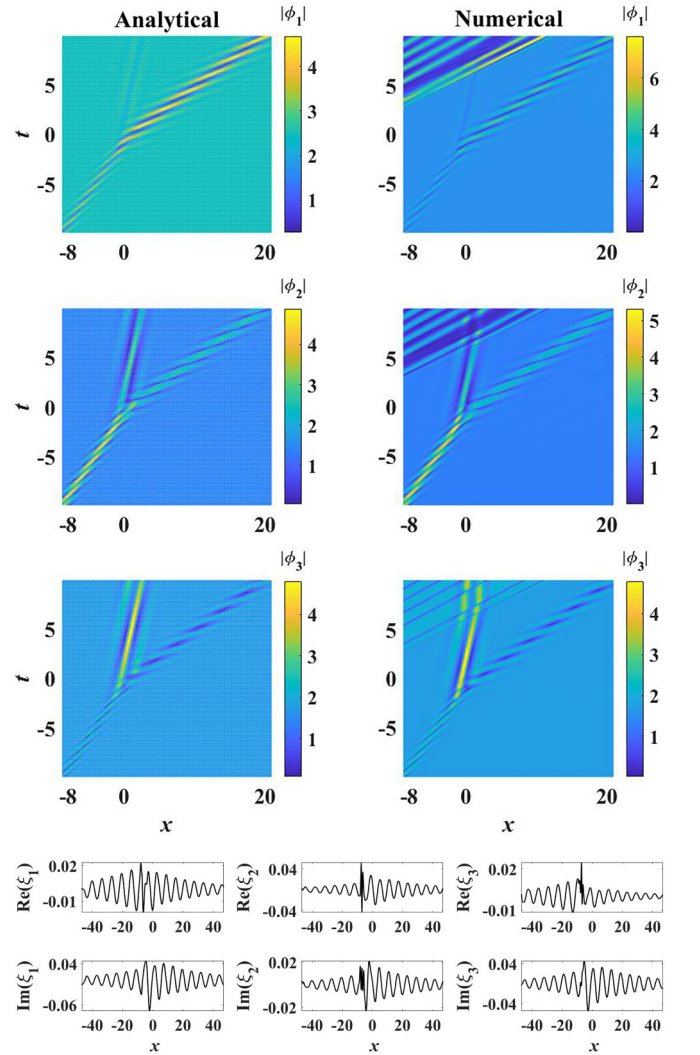

FIG. 12. (Top) Fission of breather; (Bottom) Eigenvectors by Floquet analysis. Parameters values: $\delta_1 = \delta_2 = \delta_3 = 1$, $k_1 = 0$, $\lambda = -1 + i$, $V_3 = 0$, $V_2 = 1$, $V_1 = 3$, $\mu = 0.01$.
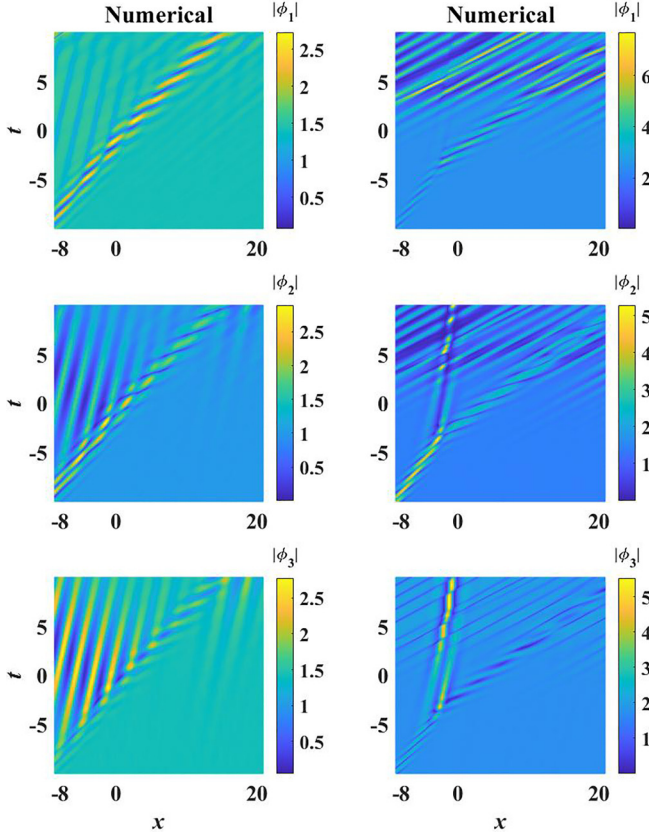
FIG. 13. Robustness test of breather fission. Parameters: $\delta_1 = \delta_2 = \delta_3 = 1$, $k_1 = 0$, $\lambda = -1 + i$, $V_3 = 0$, $V_2 = 1$, $V_1 = 2$ (left); $V_1 = 3$ (right), $\mu = 0.01$.

is obtained. Equation (32) can then be rewritten as

$$
\begin{bmatrix}
\xi_{1R}(x,\ T) \\
\xi_{1I}(x,\ T) \\
\xi_{2R}(x,\ T) \\
\xi_{2I}(x,\ T) \\
\xi_{3R}(x,\ T) \\
\xi_{3I}(x,\ T)
\end{bmatrix}
= H
\begin{bmatrix}
\xi_{1R}(x,\ 0) \\
\xi_{1I}(x,\ 0) \\
\xi_{2R}(x,\ 0) \\
\xi_{2I}(x,\ 0) \\
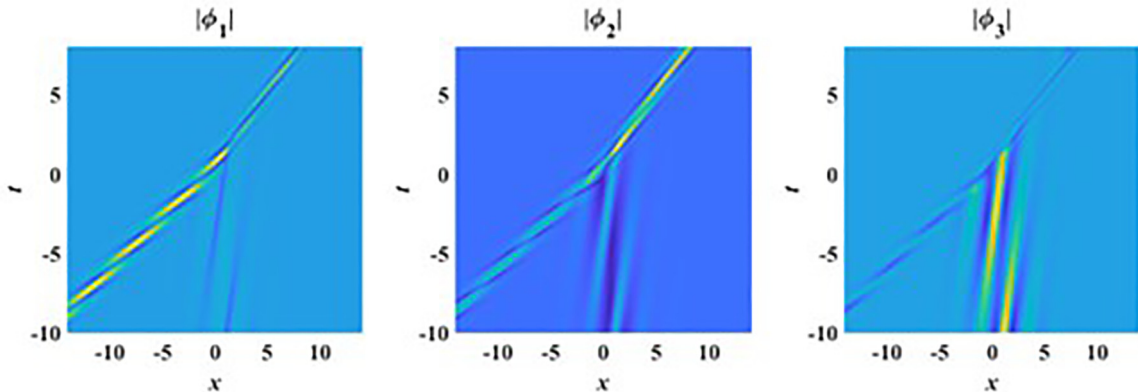\xi_{3R}(x,\ 0) \\
\xi_{3I}(x,\ 0)
\end{bmatrix}.
\tag{37}
$$

To associate the Floquet analysis with the robustness test of the breather fission, we implement the split-step Fourier method [41] and select

$$
\begin{aligned}
\phi_1(x, t_0) &= \phi_{1,\mathrm{bre}}(x, t_0) + \mu\,\zeta_1, \\
\phi_2(x, t_0) &= \phi_{2,\mathrm{bre}}(x, t_0) + \mu\,\zeta_2, \\
\phi_3(x, t_0) &= \phi_{3,\mathrm{bre}}(x, t_0) + \mu\,\zeta_3,
\end{aligned}
\tag{38}
$$

As the initial condition starting from $t_0 = -10$, where μ is the perturbation intensity, ζ_1, ζ_2, ζ_3 are denoted by ξ_1, ξ_2, ξ_3, respectively, for the Floquet analysis. For the robustness test, they will be taken as random noise to start the numerical integration. The numerical schemes and the parameters employed in the simulations will be described. The linear part of the governing equation is solved in Fourier space, and the nonlinear portion is computed by a fourth-order Runge-Kutta method. The integration of Eq. (11) is performed within the spatial box $[-L/2,\ L/2]$, where $L = 30\pi$, using a grid consisting of $N = 512$ nodes. This setting will imply a grid size of $\Delta x = L/N$. The evolution interval is taken as $[-10, 10]$ with a discretized step size of 5×10^{-4}. The eigenvectors ξ_1, ξ_2, ξ_3, can be computed from Eq. (37). The eigenvectors for the case of breather fission with $V_1 = 2$ are shown in the bottom panel of Fig. 11. The numerical breather fission phenomenon is presented in the right column of Fig. 11. Figure 12 displays the analytical and numerical breather fission for the case of $V_1 = 3$. Comparing with the case of $V_1 = 2$, we can see that the breather fission is more unstable with $V_1 = 3$. And the amplitudes of the eigenvectors with $V_1 = 3$ are larger than those of $V_1 = 2$. This may cause the breather fission phenomenon to be more pronounced for the case of $V_1 = 3$.

Next, we choose ζ_1, ζ_2, ζ_3 as the random noise subjected to a Gaussian distribution. The numerical breather fission phenomena are shown in Fig. 13, where the left column represents the numerical simulations with the case of $V_1 = 2$, while the right column corresponds to the case of $V_1 = 3$. Comparing the two cases, we observe that the breather fission for the case of $V_1 = 3$ is more unstable than that of $V_1 = 2$, which conforms with the prediction by Floquet analysis. Floquet analysis thus proves to be a reliable indicator for predicting the robustness test. For breather fusion, the qualitative trend is similar.
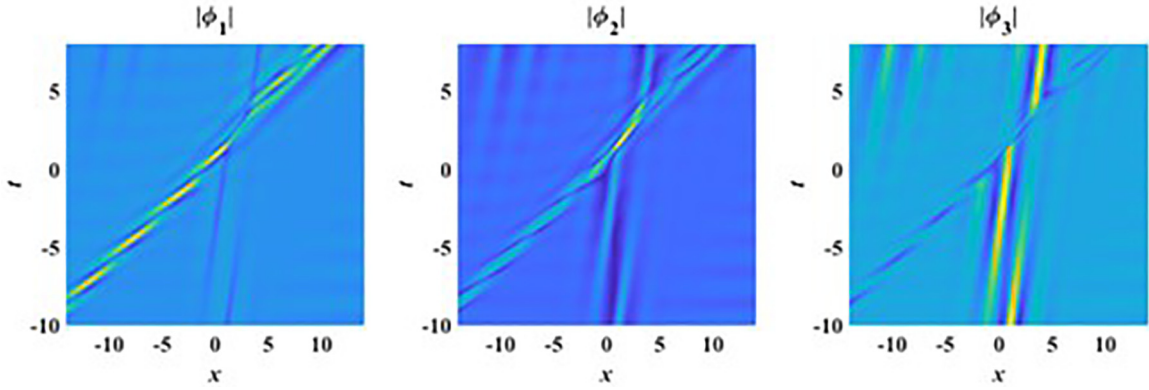

FIG. 14. Fusion of breathers with parameters $\lambda = -2 - 2i$, $V_3 = 0$, $V_2 = 1$, $V_1 = 1.8$.

FIG. 15. Cessation of the fusion process under a 10% long wave disturbance ($0.1 \sin 0.1x$).

C. Robustness test

The robustness of the breather fusion and fission processes is examined by introducing small disturbances to the analytical breather solution at a time instant just before the actual occurrence of these processes. Numerical simulations are performed using a pseudospectral method [41] with a marching forward in time starting at $t = -10$. We employ the Fourier spectral method in the spatial domain and the fourth-order Runge-Kutta method in the temporal domain for the computations.

For the fusion process, we first illustrate the exact solution graphically as a benchmark (Fig. 14). Moderate amplitude (10%) disturbances of long as well as finite wavelength are now imposed. We also test the case of random noise as a perturbation. For long wavelength (wave number = 0.1) sinusoidal disturbance, the fusion process ceases (Fig. 15). Similar conclusions apply to the case of a finite wavelength (wave number = 0.5) case as well as random noise. The two breathers appear to continue with their own propagation pathways instead of undergoing a merger. There is a phase shift after the collision.

The trend is opposite for the fission process. The exact solution is first given as a benchmark reference (Fig. 16). We again impose a moderate amplitude (10%) disturbance of long wavelength (Fig. 17). The shape of the fission process is relatively well preserved. Similar trends are observed for the scenarios of finite wavelength perturbations and random noise. Hence we can conclude that the fission process is ro-

bust, quite unlike fusion case. Furthermore, the fission process may occur earlier than the time necessary for the corresponding situation without noise.

V. DISCUSSIONS AND CONCLUSIONS

We investigate energy transfer mechanisms among oscillatory modes using fluid mechanics as a case study. Similar mechanisms should apply to optics, plasma and other fields, provided that the linear dispersion allows the existence of degenerate triads. For wave propagation in hydrodynamics, the Korteweg–de Vries or the nonlinear Schrödinger equations have been well established as canonical governing models for the long wave or finite wavelength regimes respectively [2,42,43]. However, special physical configurations typically may require previously neglected factors to be restored. For long waves in a two-layer fluid, special combinations of depth and density ratios will cause the quadratic nonlinearity to vanish. Cubic nonlinearity must be restored, leading to the modified Korteweg–de Vries equation [44]. Similarly, weakly nonlinear, narrow-band, slowly varying packets propagating over a sloping seafloor toward the shore will eventually pass through the critical point of $k_0 h_0 = 1.363$, where k_0, h_0 are the wave number of the carrier packet and water depth, respectively. Incorporating quintic nonlinearity into a higher order Schrödinger equation will clarify the dynamics on whether the packet can reach the shore [45]. In the present work, we have identified another special case relevant to ocean science
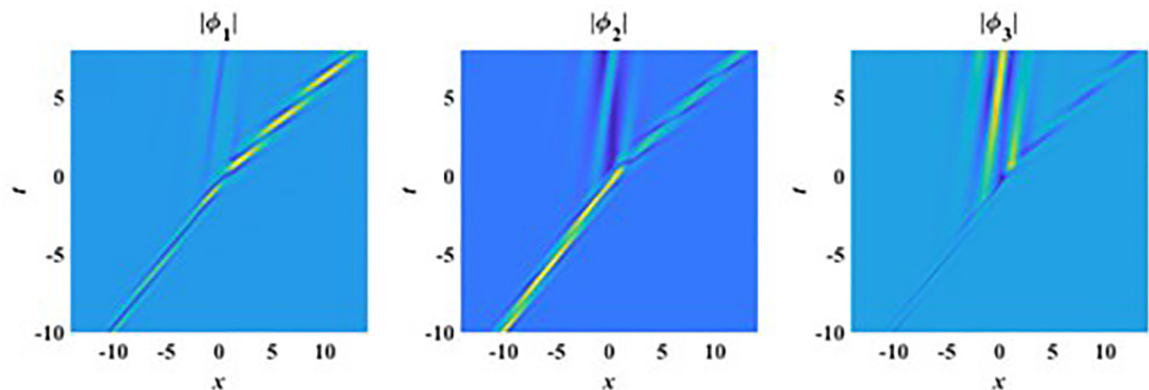

FIG. 16. Fission of breather with parameters $\lambda = -2 + 2i$, $V_3 = 0$, $V_2 = 1$, $V_1 = 1.8$.
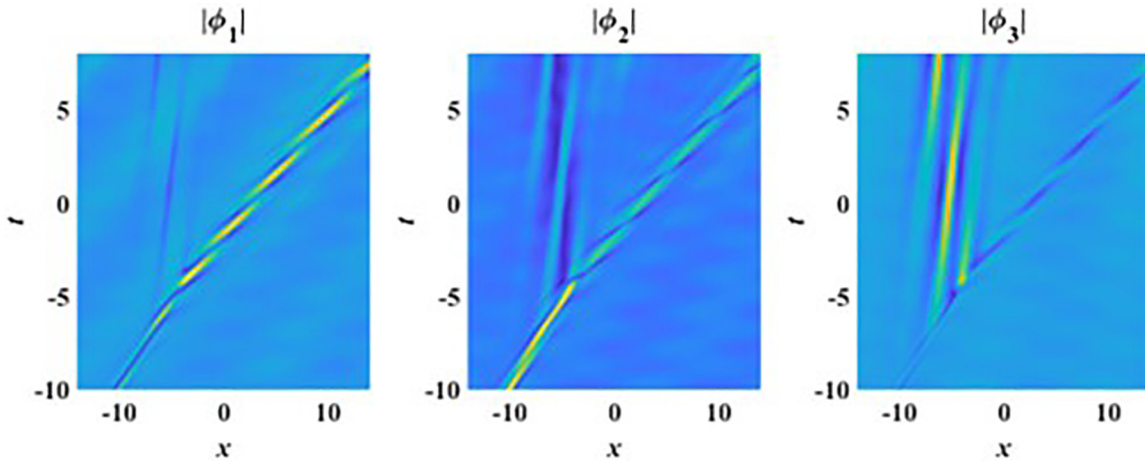
FIG. 17. Fission of breather persisting under a long wavelength perturbation $(0.1 \sin 0.1x)$.

and marine engineering, namely, triadic resonance for internal waves in a uniformly stratified fluid.

More precisely, when two of the three group velocities in a triad resonance are identical, the governing system cannot be reduced mathematically to the case with three distinct group velocities. The analytic forms of the rogue waves are also different. They have been derived in the literature by the Darboux transformation. Whether other methods like the inverse scattering transform or Hirota bilinear technique can be applied are still open questions. We elucidate the connections between the phase of the rogue waves and the points of maximum or minimum displacements. The volume of the rogue waves, defined as a measure of fluid displacement during the entire motion of the rogue mode, is an instructive quantity. As one illuminating example, this volume can increase dramatically

when the angular frequencies of two of carrier packets are close to each other.

Finally, we undertake a study on pulsating modes (breathers) in the internal wave context. Such breathers can be generated due to the decay of long tidal waves [46]. Interactions of these pulsating modes can affect the extrema, spectra, and statistical moments of the wave field, and have been studied numerically. Similarly, interactions and collisions of breathers can also occur for layered fluids [47]. Instead of using the modified Korteweg–de Vries equation, we show that employing a triad resonance model may be equally beneficial. We use the Darboux transformation to derive analytically breather (pulsating) modes. The Floquet theory of differential equations with periodic coefficients is employed to investigate
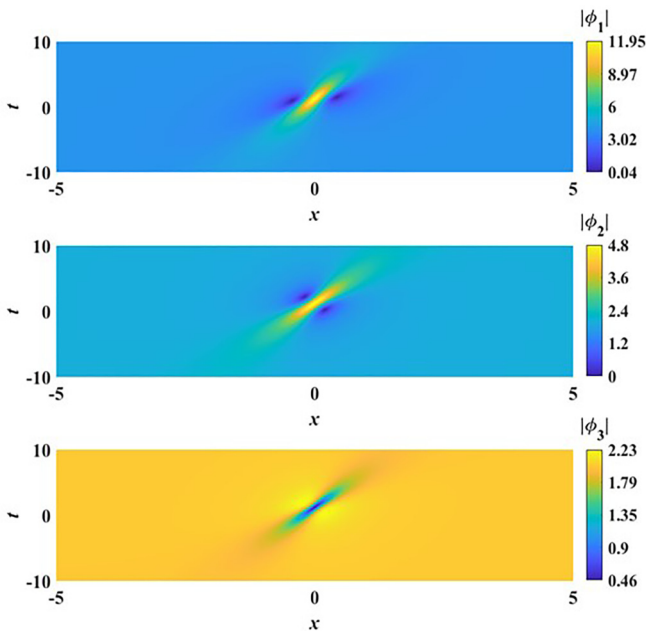

FIG. 18. Rogue waves for the nondegenerate triad system: All three components ($|\phi_1|$, $|\phi_2|$, $|\phi_3|$) display eye-shape pattern (parameters of background plane waves and group velocities given by $a_2 = a_3 = 2$, $\omega_2 = 1$, $\omega_3 = 2$, $V_2 = 1$, $V_3 = 4$).
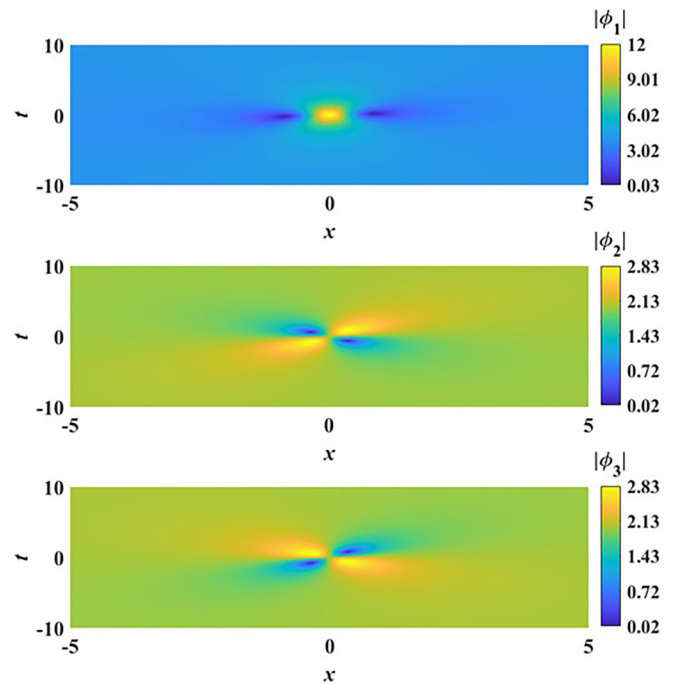

FIG. 19. Rogue waves for the degenerate triad system: $|\phi_1|$ as eye-shape but $|\phi_2|$, $|\phi_3|$ as four-petal profile [parameters: $a_2 = a_3 = 2$, $\omega_2 = 1$, $\omega_3 = 2$, $V = 4$ in Eq. (12)].

stability issues. Here the dynamics is already exceedingly complex. We just focus on the nondegenerate case in this paper. Intriguing phenomena like fission and fusion of breathers occur, similar to the situation of the nonlinear Schrödinger equations [48]. Our theory elucidates the nonlinear properties of both rogue waves and breathers, providing valuable insights in the physics of triad systems as well as applications to fluids and optics. As example, in statistically homogeneous, stationary and isotropic wave fields, low-frequency waves are mainly generated by nonlinear interactions. Triad resonance will likely play a significant role. A nonlinear sea state can thus be realized, in principle, in a laboratory, and results can be compared with theoretical models [49]. Analogies between rogue waves in the oceans and in optical fibers have been described in a recent review article [50]. Our present results enhance the knowledge in the special regime of degenerate triad resonance, and thus will help in practical applications and the interpretation of experimental results.

There are many issues requiring more investigations in the future. Once the fundamental principles explained here are understood, similar degenerate resonance should occur in other situations in hydrodynamics, e.g., layered fluids. Numerical simulations on the robustness of rogue waves and breathers ought to be further examined. Breathers for the degenerate case should be pursued too, both analytically as well as computationally. Other than the present work on uniformly stratified fluids, we expect that these degenerate three-wave interactions may be relevant for other flow situations too, e.g., gravity-capillary waves or even hydroelastic configurations [51,52]. Fruitful results in fluid dynamics and marine engineering are likely to be found. Indeed such principles should also be relevant for other fields of physical science too.

The authors have no conflicts to disclose.

Hui Min YIN: Methodology; Formal Analysis; Writing – original draft.

Qing PAN: Methodology; Formal Analysis; Writing – original draft.

Kwok Wing CHOW: Conceptualization; Writing – review & editing; Supervision.

The data that support the findings of this study are available from the corresponding author upon reasonable request.

APPENDIX A: COMPARISON OF ROGUE WAVE PROFILE

We consider typical values for the amplitudes of the plane wave background [$a_2 = a_3 = 2$, Eq. (12)] and angular frequencies of the slowly varying envelopes [$\omega_2 = 1$, $\omega_3 = 2$, Eq. (12)]. For the nondegenerate triad associated with these values, all three components are eye-shaped rogue wave (one peak or valley, with two valleys or peaks, respectively, on the opposite sides, Fig. 18). In contrast, for these same input parameters (a_2, a_3, ω_2, ω_3), a degenerate triad will have components displaying one in eye-shape and two in four-petal configurations (Fig. 19, four-petal = two peaks and two valleys surrounding a saddle point in the center). In terms of the actual maximum displacements, the largest amplitudes for the three components ($|\phi_1|$, $|\phi_2|$, $|\phi_3|$) are (11.95, 4.80, 2.23) for the nondegenerate case, but take on values of (12.00, 2.83, 2.83) for the degenerate case. The rogue modes of the degenerate and nondegenerate cases are thus clearly distinct from each other.

APPENDIX B: FORMULAS OF PARAMETERS IN EQ. (27)

We designate y_1, y_2, y_3 as the eigenvalues of the matrix $\mathbf{U}_0$ [Eq. (26a)], and z_1, z_2, z_3 as the eigenvectors corresponding to y_1, y_2, y_3. On obtaining the eigenvalues and the eigenvectors, we can then use widely used software such as MATHEMATICA to proceed with the computations of parameters in Eq. (27):

$$Q_j = G^{-1} z_j \exp\left[y_j x + \left(h_1 \xi_j + h_2 \xi_j^2 + h_3 \xi_j^3 \right) t \right], \quad j = 1, 2, 3, \tag{B1}$$

where

$$h_1 = \frac{4V_1^4 \lambda^4 + V_1^3 \lambda^3 (24 - 11V_2\lambda) + 4[9 + V_2\lambda(3 + V_2\lambda)]^2}{3\lambda[-54 + (V_1 - 2V_2)(2V_1 - V_2)(V_1 + V_2)\lambda^3]}$$
$$+ \frac{3V_1^2 \lambda^2 [36 + V_2\lambda(-3 + 8V_2\lambda)] - V_1\lambda[-216 + V_2\lambda(108 + V_2\lambda(9 + 11V_2\lambda))]}{3\lambda[-54 + (V_1 - 2V_2)(2V_1 - V_2)(V_1 + V_2)\lambda^3]}, \tag{B2}$$

$$h_2 = -\frac{i}{\lambda}, \quad h_3 = \frac{6[9 + 3(V_1 + V_2)\lambda + (V_1^2 - V_1 V_2 + V_2^2)\lambda^2]}{\lambda[-54 + (V_1 - 2V_2)(2V_1 - V_2)(V_1 + V_2)\lambda^3]}. \tag{B3}$$

[1] D. J. Kaup, A. Reiman, and A. Bers, Space-time evolution of nonlinear three-wave interactions. I. Interaction in a homogeneous medium, Rev. Mod. Phys. **51**, 275 (1979).

[2] A. D. D. Craik, *Wave Interactions and Fluid Flows* (Cambridge University Press, Cambridge, 1988).

[3] T. Dauxois, S. Joubaud, P. Odier, and A. Venaille, Instabilities of internal gravity wave beams, Annu. Rev. Fluid Mech. **50**, 131 (2018).

[4] D. J. Benney, A general theory for interactions between short and long waves, Stud. Appl. Math. **56**, 81 (1977).

[5] O. M. Phillips, On the dynamics of unsteady gravity waves of finite amplitude. Part 1. The elementary interactions, J. Fluid Mech. **9**, 193 (1960).

[6] F. Novkoski, C.-T. Pham, and E. Falcon, Evidence of experimental three-wave resonant interactions between two dispersion branches, Phys. Rev. E **107**, 045101 (2023).

[7] F. Haudin, A. Cazaubiel, L. Deike, T. Jamin, E. Falcon, and M. Berhanu, Experimental study of three-wave interactions among capillary-gravity surface waves, Phys. Rev. E **93**, 043110 (2016).

[8] W. Choi, M. Chabane, and T. M. A. Taklo, Two-dimensional resonant triad interactions in a two-layer system, J. Fluid Mech. **907**, A5 (2021).

[9] N. Bisht, S. Boral, T. Sahoo, and M. H. Meylan, Triad resonance of flexural gravity waves in a two-layer fluid within the framework of blocking dynamics, Phys. Fluids **34**, 116606 (2022).

[10] B. R. Sutherland and R. Jefferson, Triad resonant instability of horizontally periodic internal modes, Phys. Rev. Fluids **5**, 034801 (2020).

[11] Q. Pan, N. N. Peng, H. N. Chan, and K. W. Chow, Coupled triads in the dynamics of internal waves: Case study using a linearly stratified fluid, Phys. Rev. Fluids **6**, 024802 (2021).

[12] M. Funakoshi and M. Oikawa, The resonant interaction between a long internal gravity wave and a surface gravity wave packet, J. Phys. Soc. Jpn. **52**, 1982 (1982).

[13] C. Staquet and J. Sommeria, Internal gravity waves: From instabilities to turbulence, Annu. Rev. Fluid Mech. **34**, 559 (2002).

[14] S. Joubaud, J. Munroe, P. Odier, and T. Dauxois, Experimental parametric subharmonic instability in stratified fluids, Phys. Fluids **24**, 041703 (2012).

[15] H. H. Karimi and T. R. Akylas, Parametric subharmonic instability of internal waves: Locally confined beams versus monochromatic wavetrains, J. Fluid Mech. **757**, 381 (2014).

[16] H. H. Karimi and T. R. Akylas, Near-inertial parametric subharmonic instability of internal wave beams, Phys. Rev. Fluids **2**, 074801 (2017).

[17] B. Fan and T. R. Akylas, Instabilities of finite-width internal wave beams: From Floquet analysis to PSI, J. Fluid Mech. **913**, A5 (2021).

[18] T. R. Akylas and C. Kakoutas, Stability of internal gravity wave modes: From triad resonance to broadband instability, J. Fluid Mech. **961**, A22 (2023).

[19] K. M. Grayson, S. B. Dalziel, and A. G. W. Lawrie, The long view of triadic resonance instability in finite-width internal gravity wave beams, J. Fluid Mech. **953**, A22 (2022).

[20] K. Dysthe, H. E. Krogstad, and P. Müller, Oceanic rogue waves, Annu. Rev. Fluid Mech. **40**, 287 (2008).

[21] A. K. Dhar and J. T. Kirby, Fourth-order stability analysis for capillary-gravity waves on finite-depth currents with constant vorticity, Phys. Fluids **35**, 026601 (2023).

[22] M. L. McAllister, S. Draycott, T. A. A. Adcock, P. H. Taylor, and T. S. van den Bremer, Laboratory recreation of the Draupner wave and the role of breaking in crossing seas, J. Fluid Mech. **860**, 767 (2019).

[23] R. Grimshaw, E. Pelinovsky, T. Taipova, and A. Sergeeva, Rogue internal waves in the ocean: Long wave model, Eur. Phys. J.: Spec. Top. **185**, 195 (2010).

[24] B. R. Sutherland, *Internal Gravity Waves* (Cambridge University Press, Cambridge, 2010).

[25] K. Terletska, K. T. Jung, T. Talipova, V. Maderich, I. Brovchenko, and R. Grimshaw, Internal breather-like wave generation by the second mode solitary wave interaction with a step, Phys. Fluids **28**, 116602 (2016).

[26] K. G. Lamb, O. Polukhina, T. Talipova, E. Pelinovsky, W. Xiao, and A. Kurkin, Breather generation in fully nonlinear models of a stratified fluid, Phys. Rev. E **75**, 046306 (2007).

[27] R. Grimshaw, E. Pelinovsky, and T. Talipova, Fission of a weakly nonlinear interfacial solitary wave at a step, Geophys. Astrophys. Fluid Dyn. **102**, 179 (2008).

[28] V. V. Voronovich, I. A. Sazonov, and V. I. Shrira, On radiating solitons in a model of the internal wave–shear flow resonance, J. Fluid Mech. **568**, 273 (2006).

[29] F. Baronio, M. Conforti, A. Degasperis, and S. Lombardo, Rogue waves emerging from the resonant interaction of three waves, Phys. Rev. Lett. **111**, 114101 (2013).

[30] G. Zhang, Z. Yan, and X. Y. Wen, Three-wave resonant interactions: Multi-dark-dark-dark solitons, breathers, rogue waves, and their interactions and dynamics, Physica D **366**, 27 (2018).

[31] B. Yang and J. Yang, General rogue waves in the three-wave resonant interaction systems, IMA J. Appl. Math. **86**, 378 (2021).

[32] S. Chen, F. Baronio, J. M. Soto-Crespo, P. Grelu, and D. Mihalache, Versatile rogue waves in scalar, vector, and multidimensional nonlinear systems, J. Phys. A **50**, 463001 (2017).

[33] H. M. Yin, Q. Pan, and K. W. Chow, Four-wave mixing and coherently coupled Schrödinger equations: Cascading processes and Fermi-Pasta-Ulam-Tsingou recurrence, Chaos **31**, 083117 (2021).

[34] G. Xu, K. Hammani, A. Chabchoub, J. M. Dudley, B. Kibler, and C. Finot, Phase evolution of Peregrine-like breathers in optics and hydrodynamics, Phys. Rev. E **99**, 012207 (2019).

[35] N. Devine, A. Ankiewicz, G. Genty, J. Dudley, and N. Akhmediev, Recurrence phase shift in Fermi-Pasta-Ulam nonlinear dynamics, Phys. Lett. A **375**, 4158 (2011).

[36] A. Ankiewicz, Rogue and semi-rogue waves defined by volume, Nonlinear Dyn. **104**, 4241 (2021).

[37] M. Romano, S. Lombardo, and M. Sommacal, The 3-wave resonant interaction model: Spectra and instabilities of plane waves, Z. Angew. Math. Phys. **74**, 203 (2023).

[38] H. M. Yin and K. W. Chow, Fermi-Pasta-Ulam-Tsingou recurrence and cascading mechanism for resonant three-wave interactions, Phys. Rev. E **107**, 064215 (2023).

[39] G. Mu and Z. Qin, High order rational solitons and their dynamics of the 3-wave resonant interaction equation, Physica D **435**, 133287 (2022).

[40] J. Cuevas-Maraver, P. G. Kevrekidis, D. J. Frantzeskakis, N. I. Karachalios, M. Haragus, and G. James, Floquet analysis of Kuznetsov-Ma breathers: A path towards spectral stability of rogue waves, Phys. Rev. E **96**, 012202 (2017).

[41] Jianke Yang, *Nonlinear Waves in Integrable and Nonintegrable Systems* (SIAM, Philadelphia, 2010).

[42] K. W. Chow, R. H. J. Grimshaw, and E. Ding, Interactions of breathers and solitons in the extended Korteweg–de Vries equation, Wave Motion **43**, 158 (2005).

[43] A. Chabchoub, N. Hoffmann, E. Tobisch, T. Waseda, and N. Akhmediev, Drifting breathers and Fermi-Pasta-Ulam paradox for water waves, Wave Motion **90**, 168 (2019).

[44] T. Kakutani and N. Yamasaki, Solitary waves in a two-layer fluid, J. Phys. Soc. Jpn. **45**, 674 (1978).

[45] R. H. J. Grimshaw and S. Y. Annenkov, Water wave packets over variable depth, Stud. Appl. Math. **126**, 409 (2011).

[46] E. Didenkulova and E. Pelinovsky, Interaction features of internal wave breathers in a stratified ocean, Fluids **5**, 205 (2020).

[47] K. Nakayama and K. G. Lamb, Breather interactions in a three-layer fluid, J. Fluid. Mech. **957**, A22 (2023).

[48] H.-M. Yin, B. Tian, and X.-C. Zhao, Chaotic breathers and breather fission/fusion for a vector nonlinear Schrödinger equation in a birefringent optical fiber or wavelength division multiplexed system, Appl. Math. Comput. **368**, 124768 (2020).

[49] G. Michel, F. Bonnefoy, G. Ducrozet, and E. Falcon, Statistics of rogue waves in isotropic wave fields, J. Fluid. Mech. **943**, A26 (2022).

[50] J. M. Dudley, G. Genty, A. Mussot, A. Chabchoub, and F. Dias, Rogue waves and analogies in optics and oceanography, Nat. Rev. Phys. **1**, 675 (2019).

[51] Q. Aubourg and N. Mordant, Investigation of resonances in gravity-capillary wave turbulence, Phys. Rev. Fluids **1**, 023701 (2016).

[52] L. Deike, M. Berhanu, and E. Falcon, Experimental observation of hydroelastic three-wave interactions, Phys. Rev. Fluids **2**, 064803 (2017).